Comparing Chemical Compositions of Dwarf Elliptical Nuclei and Globular Clusters

Abstract

Because of their abundance in cluster environments and fragility due to their low mass, dwarf elliptical galaxies (dEs) are excellent specimens for studying the physical processes that occur inside galaxy clusters. These studies can be used to expand our understanding of the process of galaxy (specifically dE) formation and the role of dark matter in the Universe. To move closer to better understanding these topics, we present a study of the relationship between dEs and globular clusters (GCs) by using the largest sample of dEs and GC satellites to date. We focus on comparing the ages and chemical compositions of dE nuclei with those of satellite GCs by analyzing absorption lines in their spectra. To better view the spectral features of these relatively dim objects, we employ a spectral co-addition process, where we add the fluxes of several objects to produce a single spectrum with high signal-to-noise ratio. Our finding that dE nuclei are younger and more metal rich than globular clusters establishes important benchmarks that future dE formation theories will consider. We also establish a means to identify GCs whose parent galaxies are uncertain, which allows us to make comparisons between this GC group and the satellite GCs.

1. Introduction

1.1 Dark Matter in Cluster Environments

Cluster environments are regions of the Universe where galaxies exist in close proximity to one another and are held together by the gravitational pull of luminous and dark matter, a type of matter that neither emits nor absorbs light. The Universe is currently thought to be composed of 96% dark matter; yet astronomers know very little about its composition, formation, and origins. Since this substance cannot be observed directly, we must rely on its gravitational influence on other objects to characterize it. One group of objects ideal for this analysis is dwarf elliptical galaxies, as they are thought to contain large amounts of dark matter.

1.2 Dwarf Ellipticals in Cluster Environments

Dwarf elliptical (dE) galaxies are the most abundant type of galaxy in cluster environments (Dressler 1980, Binggeli, Sandage & Tammann 1985, Binggeli et al. 1988). Because of their low luminosity (blue magnitude fainter than -18) and therefore lower mass, dEs are more susceptible to the effects of a cluster environment than larger galaxies. This quality makes them key "laboratories" for examining different galaxy-shaping processes and the role of dark matter in them.

Since the discovery of dwarf ellipticals, astronomers have struggled to characterize their formation. Near the time that they were first discovered, research showed that dEs were closely related to massive ellipticals because of the similar smooth structures they shared (Ferguson & Binggeli 1994). Later, however, researchers learned that such a postulate was only supported in scenarios where galaxies are round and pressure supported, conditions which were only present near the center of clusters (Toloba et al. 2009, 2011, 2014). A new formation process was proposed: dEs are late-type galaxies that fell into a cluster environment and experienced environmental distortion and other effects (Bender, Burstein & Faber 1992).

A majority of bright dwarf ellipticals contain a high luminosity center that is known as the nucleus of the galaxy (Ferguson & Binggeli 1994, Côté et al. 2006). These nuclei are typically 20 percent more luminous than the remainder of their galaxy. (Ferguson & Binggeli 1994, Côté et al. 2006). In this project, we aim to further understand the dE nuclei's relation to globular clusters (GCs), or dense families of old stars. Many theories regarding the origin of these bright nuclei exist. One such theory is dynamical friction, which proposes that dE nuclei might be composed of GCs that were pulled from their orbit around the dE into its center (Oh et al. 2000). While GCs are bright and easily observable, they are also important lenses into early processes of galaxy formation (Peng et al. 2006).

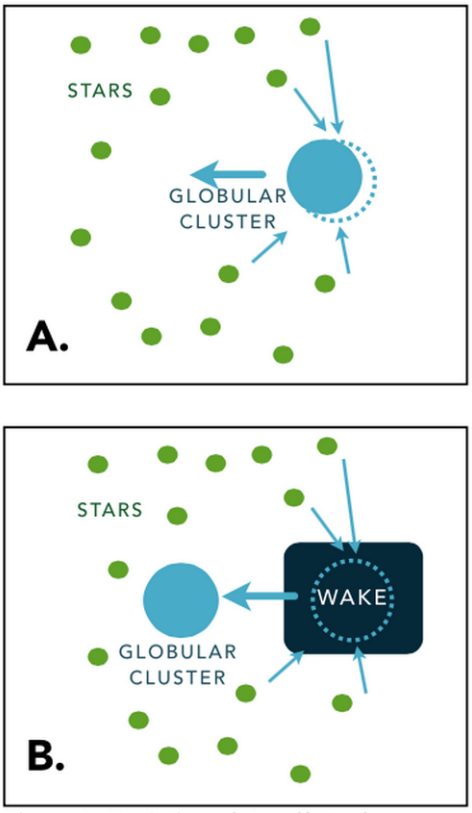

Figure 1: Depiction of the effect of dynamical friction. As the GC (blue circle) moves from right to left, the stars and other objects (green dots) in the galaxy that are gravitationally attracted to the GC leave behind a gravitational wake that causes the GC to slow down and possibly spiral into the center.

When a GC orbits its parent dE, there exist two points of gravitational pull: one at the center of the galaxy, that attracts the GC; and one at the center of the GC, that attracts stars and other objects in the main body of the parent dE galaxy. If the globular cluster were stationary, the objects it attracts would be directly attracted to it, creating an even larger cluster (Figure 1A); however, the GC is in motion. By the time the stars have responded to the gravitational attraction of the GC, the GC has already moved on, thus creating a gravitational wake behind the GC as seen in Figure 1B. This wake slows down the GC's motion, decaying its orbit around the galaxy and possibly causing it to spiral into the center of the dE. This suggests that dE nuclei may be composed of many former GCs (Oh et al. 2000).

1.3 Spectra

To find possible evidence of dynamical friction in dEs, our project compares the spectral characteristics of GCs still in orbit with the characteristics of GCs whose orbits have decayed to form the dE nucleus. We focus on the similarities and differences in the spectral properties of 19 nuclei and 128 GCs in the Virgo Cluster, the first spectral comparison of such magnitude. For this analysis, we apply a method called spectral co-addition in which the fluxes of several objects are added together to enhance spectral features and increase the signal-to-noise ratio, enabling us to make more accurate comparisons among usually faint and noisy spectra. Our study, focused on the absorption lines of hydrogen and metals in the co-added spectra of dEs and GCs, reveals age and metallicity relationships of both objects, which will provide and us with new insight into dE formation theories and benchmarks for future theories.

Furthermore, our project establishes a method for identifying GCs whose parent galaxy is not a dE, but most likely the massive elliptical M87 in the center of Virgo. This method allows us to make comparisons between the spectra of dE-bounded GCs and other GCs, enhancing our understanding of GCs in the formation of other galaxies.

2. Methods

All spectroscopic data for this study were collected using the Deep Imaging Multi-Object Spectrograph (DEIMOS). Photometric data were obtained from the Next Generation Virgo Survey (NGVS) in combination with the Advanced Camera for Surveys Virgo Cluster Survey (ACSVCS), a Hubble Space Telescope program that imaged 100 early-type galaxies in the Virgo Cluster (Côté et al. 2004, Ferrarese et al. 2012). First, we used broadband color data to assess sample contamination and identify orphan GCs; next, we employed a process called spectral co-addition, in which we added the fluxes of our dEs and GCs together, respectively.

2.1 Data Overview

This sample of GCs around dEs is the most accurate and uniform that currently exists. GCs selected to be part of our sample were located as far as 5 to 15 effective radii from the dE nuclei, regions that would be difficult to observe without the presence of bright GCs. After reducing our sample by removing objects with low redshift confidences, we obtained spectral data from 83 GC satellites gravitationally bound to an identified dE, and 45 "orphan" GCs, whose parent galaxy is uncertain but suspected to be the massive elliptical galaxy M87 in Virgo.

DEs selected to be part of our sample had lower luminosities than former studies with violet magnitudes of $-17 < \mathrm{M}_V < -15$.

2.2 Identifying "Orphan" Globular Clusters

Because globular clusters look very similar to stars, it is often difficult to differentiate between the two. Especially when GCs are not bound to a known dwarf elliptical and are therefore not clustered in more visible groups, they are drowned out in a sea of numerous stars. In this section we discuss a method for identifying these orphan GCs as well as accounting for stellar contamination in our GC sample.

2.2.1 Color-Color Diagrams

The first step in finding orphan GCs was to determine if any objects in our sample were contaminants; that is, we needed to determine whether some GCs within our sample were in fact stars simply "posing" as a GC. To carry out this process we looked at the position of GCs, both satellite and orphans, in color-color space using color-color diagrams (2CDs).

Objects are assigned a possible object classification (GC or star) based on their velocities. An object in the velocity range of -3000 km/s to 3000 km/s is defined as a GC candidate; an object in the range of -300 km/s to 300 km/s is defined as a Milky Way star candidate. Since Milky Way stars and GCs can often be similar in size, color, and luminosity, they can be difficult to distinguish. Thus, in the overlapping region of the velocity ranges of the two objects, object

classification can be incorrect, resulting in a potentially ambiguous classification.

For objects with secure velocities, we plotted objects' ultraviolet - green (u - g) color vs green - far red (g - z) color. As seen in Figure 2, some overlap between objects with GC-like and star-like velocities between ~0.6 g - z and ~1.2 g - z exists, suggesting that some GCs might actually be stars and vice versa. (Note: "color" in this context refers to the difference in magnitudes of the measurements of light through various filters such as green, ultraviolet, and far red.)

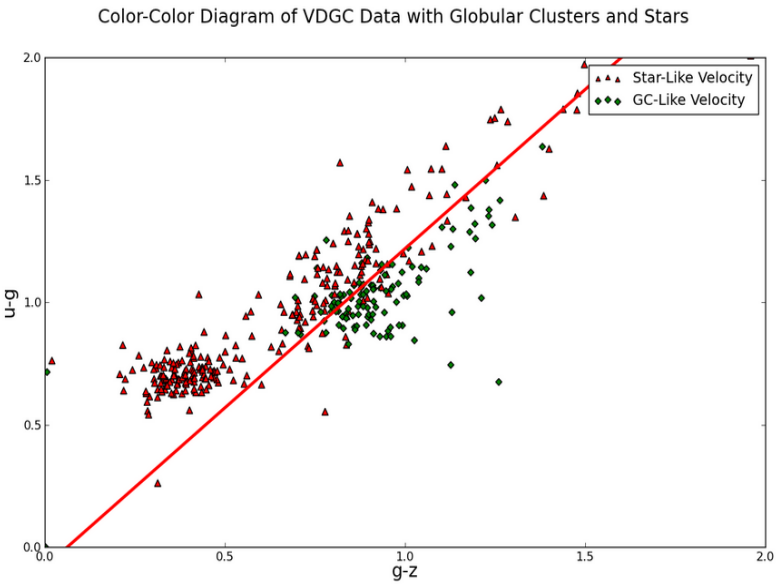

Figure 2: Color-color diagram (2CD). 2CD of objects with star-like or GC-like velocities in u - g vs g - z color. Notable knots of GCs and stars mixed together exist between ~0.6 and 1.2 g - z, indicating ambiguity in object classification and contamination. It is important to assess to what degree these regions are contaminated before performing further steps of GC analysis. The red line along the stellar sequence divides the data into above-line and below-line samples.

Next, we plotted a line parallel to the stellar sequence onto our 2CD (seen in red in Figure 2) to divide the GC sample into two data sets (above and below the line). Since the GC sample above the line lies in the same color-color space of foreground stars, some of the supposed GCs may really be contaminant stars. To confirm our prediction, we created and compared cumulative velocity histograms of these two GC groups.

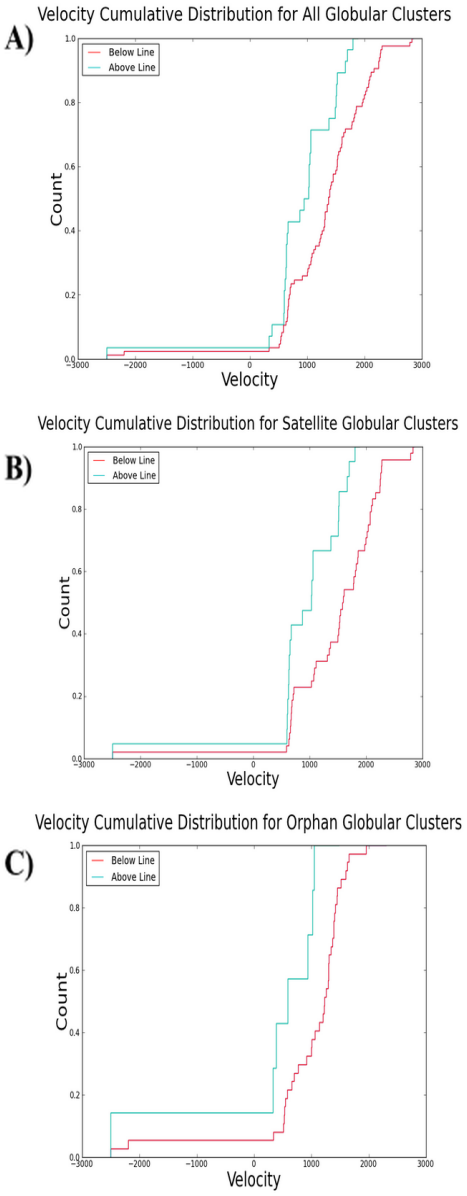

Figure 3: Velocity histograms. Cumulative velocity histograms of all GCs in 3A, only satellites in 3B, and only orphans in 3C. Each of these graphs have two histograms, one for the above-line sample and another for the below-line samples.

2.2.2 Cumulative Velocity Histograms

Cumulative velocity histograms allowed us to compare the different distributions of velocity above and below the line for both orphan and satellite GCs. We created velocity histograms that analyzed contamination in the GC sample (stars that were misclassified as GCs). First, as seen in Figure 3A, we plotted two cumulative velocity histograms of all GCs above and below the line and within the g - z range of 0.65 to 1.5. We repeated the same process for only satellite GCs as shown in Figure 3B.

Afterwards, we isolated all orphan GCs in the samples from above and below the line, plotting the distributions of both samples individually in Figure 3C. Similar distributions in the above and below line samples would indicate that both are quite similar with few contaminants; two very different distributions, however, would indicate potential misclassification because objects above the line line greatly vary in velocity from objects below the line.

2.2.3 Kolmogorov-Smirnov Statistical Test

For a statistical way that specifically analyzed the difference in our sample distributions, we conducted a Kolmogorov-Smirnov (K-S) test to compare the velocities of GCs above and below the line. The K-S test returns a p-value that assesses the probability that the two distributions come from the same parent sample. If this p-value is lower than the 3-sigma limit of 0.003 (99.7% probability), then the difference in the distribution is significant, indicating that the velocity distribution is significantly different between the two samples.

When applying the K-S test to the velocity distributions of all GCs above and below the line, we found that the p-value was lower than the 3-sigma limit, indicating that the samples were likely to have come from two different distributions. At first glance, this K-S test result and differences in the velocity histogram distributions imply considerable contamination in our GC sample; however, upon closer review, this is not the case.

In Figure 3A, we saw several spikes in the GC sample above the line at ~600 km/s, 900km/s, and 1300km/s, which were causing the disparity in velocity distributions. After splitting the satellite and orphan GCs into two sets of velocity distributions, we found that a group of satellite GCs with almost identical velocities caused those spikes in Figure 3B, demonstrating that the origin of these spikes is in the satellite GC sample. This finding seems logical, as many satellite GCs are potentially bound to the same dE and are thus expected to have very similar velocities. There also existed one spike amongst the distribution of above-line orphan GCs in Figure 3C that could be a source of contamination. Additional investigation into these objects revealed they have very close positions in the sky in addition to having similar velocities. These orphans were not incorrectly classified, but possibly satellites of another galaxy inside the Virgo Cluster, most likely M87. Further analysis is required to verify this hypothesis, but if it proves true, then these GCs would constitute the most remote sample studied, as they would be 25 to 75 effective radii out from M87's center.

2.3 Spectrum Preparation

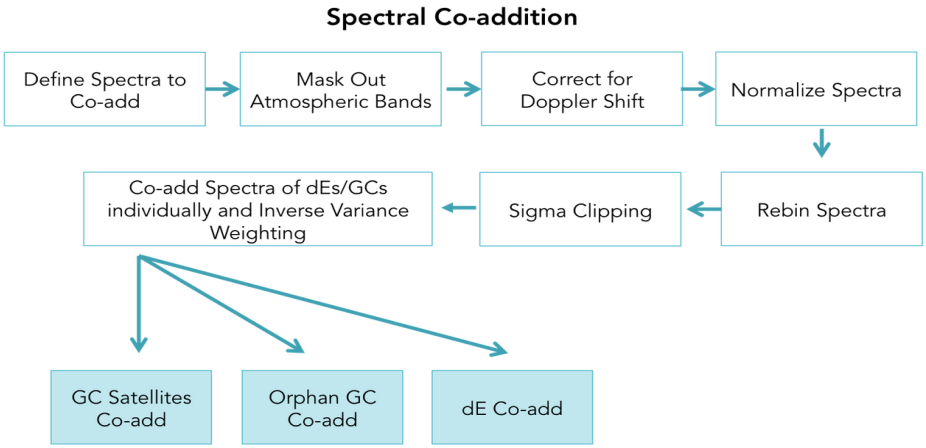

Figure 4: Overview of the steps in spectral co-addition.

After determining that most of our satellite and orphan GC samples was pure, we could proceed to safely use the spectral data of all satellites and orphans. Prior to spectral co-addition, the observed spectra from all objects need to be modified through techniques including Doppler shifting, normalization, and rebinning before any spectral analysis or co-addition can be completed.

2.3.1 Masking Out Atmospheric Bands

The absorption of some wavelengths of incoming light by molecules in the Earth's atmosphere can show absorption bands at certain spectral regions. This telluric contamination is not representative of the observed object's chemical composition, so we masked out data in the A (7585Å to 7690Å) and B (6850Å to 7015Å) atmospheric bands.

2.3.2 Doppler Shift

As objects in space move away from or towards Earth, the emitted wavelengths of light are shifted through the Doppler effect. Objects with different velocities are shifted by different amounts, meaning the observed spectra need to be adjusted to the rest frame using the equation

$\lambda_{rest} = \lambda_{obs}/(1 + \frac{v}{c})$, where λ_{rest} is the wavelength at rest frame, λ_{obs} is the original wavelength of the observed spectra, v is the velocity of the object, and c is the speed of light.

2.3.3 Normalization

The continuum, or the fundamental structure of a spectrum, primarily depends on the brightness of the object; since each star has a unique brightness, the continuum also occurs at distinct values. In order to co-add the spectra of different objects, we normalized the continuum of all objects to 1.

2.3.4 Rebinning

Another necessary component of spectrum preparation is rebinning the spectra. The observed spectra are not usually collected at uniform wavelength steps, so all objects start and end at different wavelengths and have unequal spacing in between each value. Because spectral co-addition requires all spectra to have the same wavelength set, we used a process called rebinning that redistributed fluxes to standardize these sets.

2.4 Spectral Co-addition

The spectrum of just one object, especially the inherently dim dEs we observed, can be very faint and noisy. To improve the signal-to-noise ratio (SNR) and reduce the effect of instrumental artifacts specific to certain objects, we used a technique called spectral co-addition that combines the spectral data of all objects into one reliable set. In our project, we co-added the spectra of 21 dE nuclei, 83 satellite GCs, and 45 orphan GCs.

2.4.1 Sigma Clipping

Faulty spectral data of individual objects from instrumental artifacts and cosmic rays should not be included in the co-addition. We iterated through the spectral data of each object and applied a technique called sigma clipping. At each wavelength, we determined the median flux value of all objects and compared this median to fluxes of individual objects. The fluxes more than three and a half standard deviations from the median were rejected.

2.4.2 Inverse Variance Weighting

The primary purpose of spectral co-addition is to maximize the signal-to-noise ratio and minimize the variance of the weighted average of all the fluxes. Inverse variance weighting, a method that effectively minimizes the variance, was applied to the sum of the fluxes of the sigma clipped spectra. The equation for this process is:

$$\bar{j}_i = \frac{\sum_{k=1}^{n} \frac{j_{i,k}}{\sigma_{i,k}^2}}{\sum_{k=1}^{n} \frac{1}{\sigma_{i,k}^2}} \tag{1}$$

where $j_{i,k}$ is the flux at the i-th wavelength of the j-th sigma clipped spectrum in a group of objects, $\sigma_{i,k}^2$ is the variance of $j_{i,k}$, n is the number of spectra, and $\bar{j}_i$ is the weighted average flux of the i-th wavelength.

2.4.3 Spectral Co-addition of Dwarf Elliptical Nuclei and Globular Clusters

Applying the co-addition equation on all 21 dE nuclei from 4650Å to 9300Å produced a spectrum with high SNR and clear absorption lines. Two dE nuclei were brighter than the remaining 19, meaning their SNR and inverse variances were greater as well. Because we used an inverse variance weighting technique in the co-addition, the spectral data from these two nuclei dominated the weighted average flux. Consequently, the co-added spectrum mirrored the spectra of these two nuclei and retained their unique features. To look at a spectra that was not dominated by the two brightest nuclei, we co-added only the faintest 19 nuclei. We also used Equation 1 to make two types of co-added spectra for GCs, one of the 83 satellite GCs and another of the 45 orphan GCs. Finally, we made two comparisons with our co-added spectra results. The first comparison was between the satellite GCs and the 19 faint dE nuclei and the second was between the satellite and orphan GCs.

3. Results and Discussion

3.1 Comparing the Chemical Compositions of Dwarf Elliptical Nuclei and GC Satellites

We created ladder plots that contain the co-added spectra of the 19 fainter dE nuclei and 83 GCs as well as the ratio of GC spectra to nuclei spectra. Figure 5 shows the spectra across the entire wavelength range of 4650Å to 9300Å.

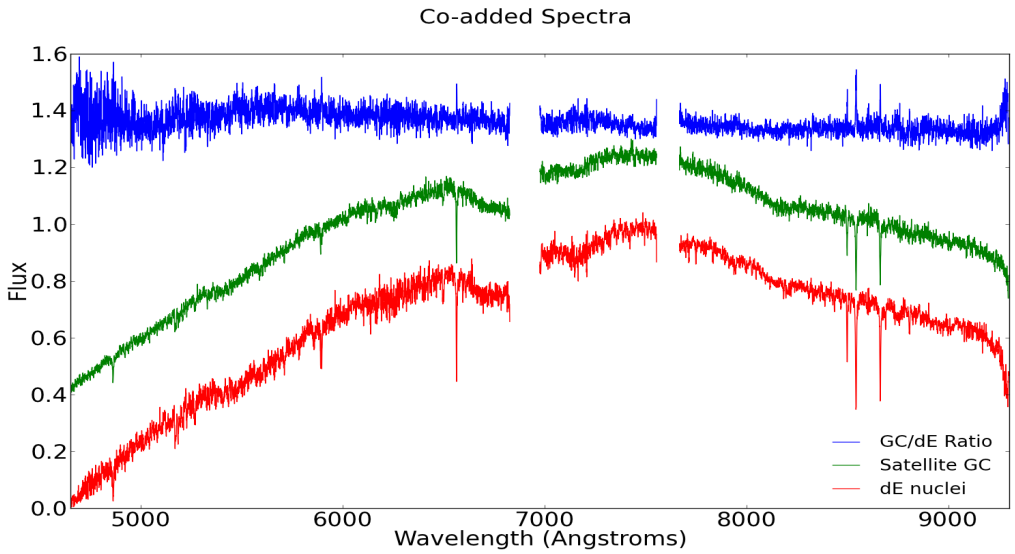

Figure 5: Co-added Spectra of dE nuclei and Satellite GCs. dE nuclei are represented in red, satellite GCs in green, and the ratio of GCs to nuclei in blue. The noticeable spikes and dips in the blue ratio are caused by differences in the GC and dE nuclei absorption lines. Note that the discontinuities in the spectra are the telluric A and B bands, which were masked out in 2.3.1.

The ratio is mostly flat (excluding at absorption lines and extreme ends of the spectrum) throughout the entire wavelength range, suggesting that the two spectra were generally similar with minor differences. To find these differences, we zoomed in on the wavelength regions of specific absorption lines and qualitatively compared the spectra. We concentrated on hydrogen lines to learn more about age and calcium, magnesium, and sodium lines to investigate the metallicity of both types of objects.

The Balmer H-alpha and H-beta are useful absorption lines to look at the age of stellar populations (Worthey et al. 1994). H-alpha and H-beta tend to be strongest in the relatively short-lived and massive A-type stars, and younger stellar populations usually contain a higher proportion of A-type stars. In both graphs of Figure 6, the dE nuclei have H-alpha and H-beta absorption lines that are slightly stronger than those of the GCs because the blue ratio has a subtle spike where the two other spectra dip. Stronger H-alpha and H-beta lines suggest that the dE nuclei are, on average, slightly younger than the satellite GCs.

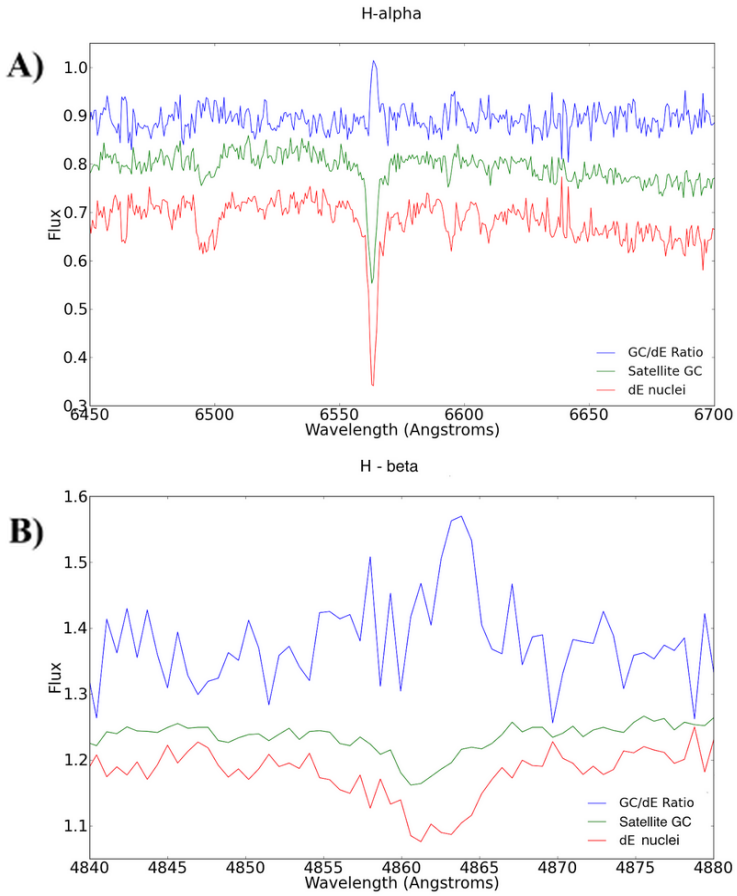

Figure 6: H-alpha and H-beta Absorption Lines. 6A shows the H-alpha absorption line (6563Å) and 6B shows the H-beta absorption line (4861Å). The H-alpha and H-beta lines of the dE nuclei dip deeper than those of the GC satellites, indicating that the nuclei are younger than the orbiting globular clusters.

Our next area of focus was using several metal absorption lines to study metallicity, or

the proportion of matter composed of elements other than hydrogen or helium. Just like the hydrogen lines, metal absorption lines that dip deeply show a high average metallicity. We first inspected the CaII Triplet (CaT) that is a good indicator of metallicity (Terlevich, Diaz & Terlevich 1990). Figure 7 showed that the CaT lines are noticeably stronger in the dE nuclei because of the pronounced spikes in the ratio at the absorption wavelengths, suggesting that the nuclei have higher average metallicities than the GCs.

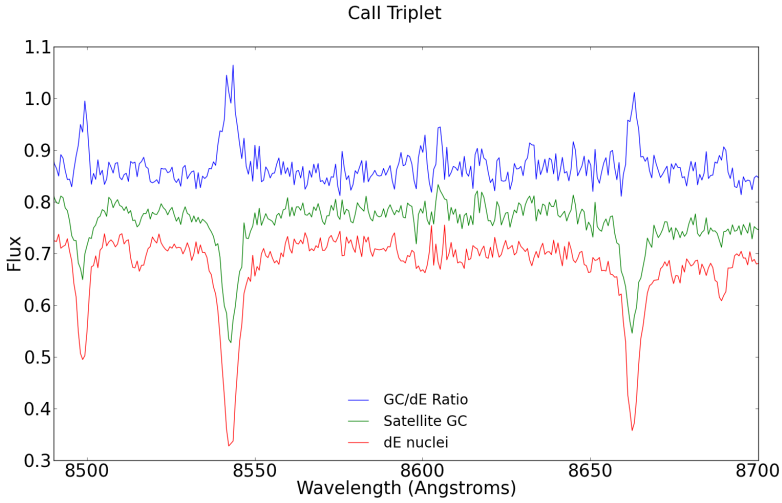

Figure 7: CaII Triplet Absorption Lines. The CaII Triplet (8498Å, 8542Å, and 8662Å) lines indicate an object's metallicity. Since CaT lines of the dE nuclei are stronger than those of the satellite GCs, the nuclei have a higher average metallicity. Another metallicity indicator in the figure is the the iron line between the first two calcium lines.

To support our CaT metallicity results, we also analyzed other metal absorption lines such as iron, magnesium, and sodium. The iron (Fe) line at 8515Å can be seen in Figure 7, but it is very weak compared to the CaT. A more zoomed in view shows that dE nuclei have slightly stronger Fe lines. Moreover, we analyzed two magnesium metallicity indicators in the magnesium triplet (MgT) around 5170Å and a single magnesium line (Mg) at 8806Å (Worthey et al. 1994, Tantalo & Chiosi 2004, Trager et al. 2008). In Figure 8A, we show that the stronger Mg line of the dE nuclei indicates higher metallicity, but the MgT lines did not have a definitive outcome in Figure 8B. The MgT nuclei absorption lines do appear stronger, but the spectra surrounding the lines

are so noisy that the ratio lacks the prominent spikes we expect to see; thus, we can confidently use the findings from the single Mg line but must be cautious deriving any conclusions from the MgT lines.

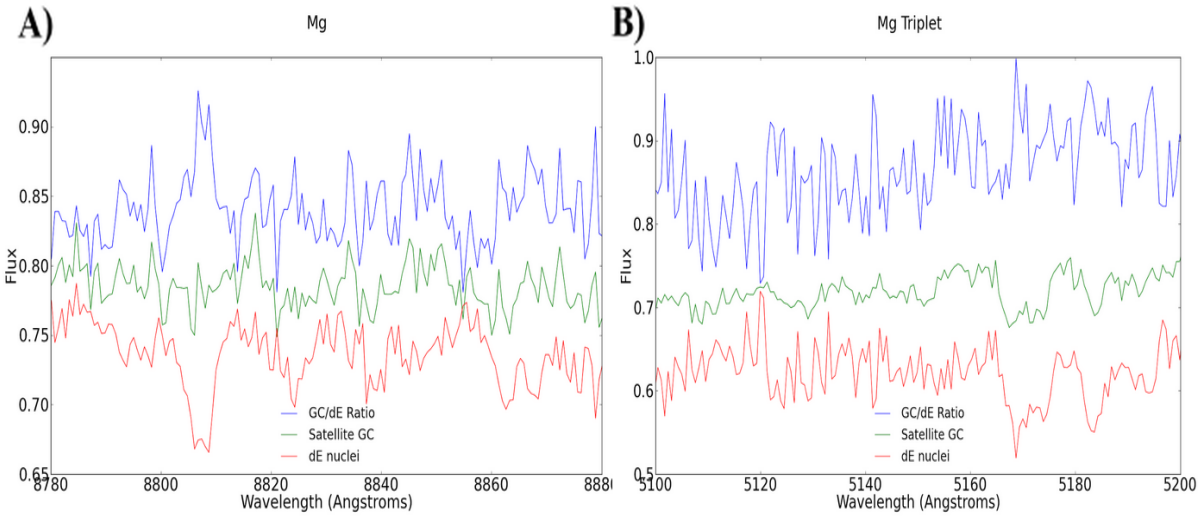

Figure 8: Magnesium Absorption Lines. 8A shows the single magnesium (Mg) line at 8806Å and 8B covers the magnesium triplet (MgT) around 5170Å. The Mg line of the dE nuclei is visibly stronger, while the MgT is too noisy to have conclusive results.

Finally, we examined two Na doublet (NaD) lines at 5890Å and 5896Å and at 8183Å and 8195Å. As shown in Figure 9B, the latter has a very flat ratio without any large spikes. On the other hand, the ratio of the other NaD lines in Figure 9A has a prominent spike, suggesting dE nuclei have higher sodium abundances, and therefore, higher metallicities. These two NaD results seem to contradict each other, but the doublet at 8183Å and 8195Å is a more sensitive indicator of the mass function, or the distribution of stellar mass, than of sodium abundance (Schiavon 1997, Cenarro et al. 2003, van Dokkum & Conroy 2011). We then focus on the NaD lines at 5890Å and 5896Å, which suggests that the nuclei have higher average metallicities than GCs. The results from the single magnesium line and one of the NaD lines consistently support our CaT findings that dE nuclei have higher metallicities than the satellite GCs.

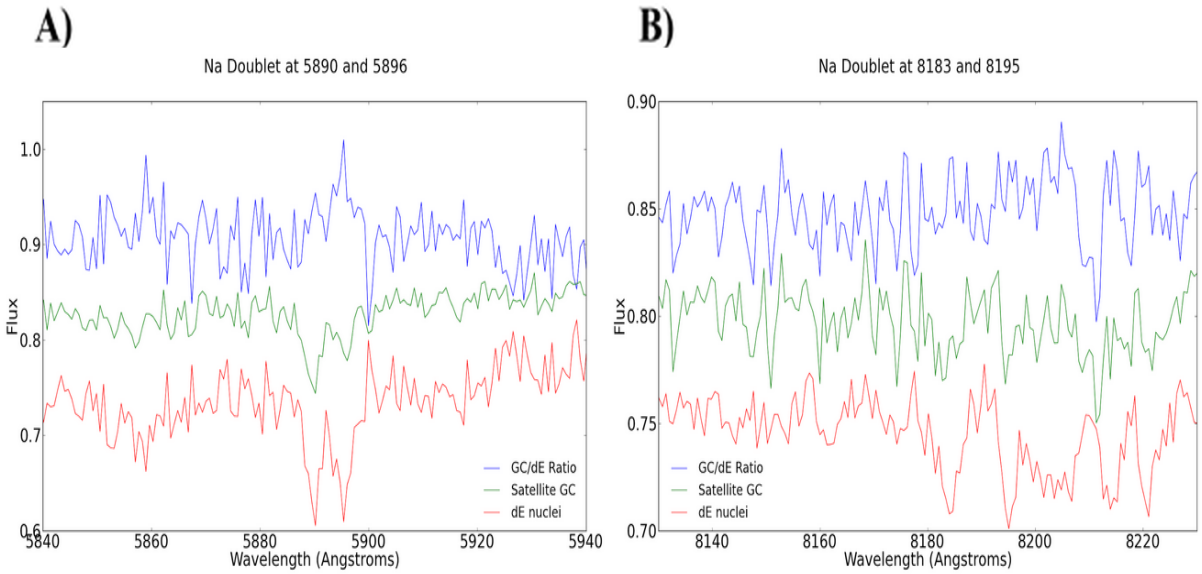

Figure 9: Two Na Doublet Absorption Lines. The Na Doublet (NaD) absorption line at 5890Åand 5896Åis visible in 9A, while 9B shows the Na Doublet (NaD) absorption lines at 8183Åand 8195Å. The former NaD line is stronger in dE nuclei than GC satellites, indicating that the nuclei have higher metal abundances.

Current theories of dE formation should consider the parameter that dE nuclei are younger with higher metallicities than the GC satellites. Assuming the dE nuclei is formed by dynamical friction, then the GCs closer to the center of the dE are the first to preferentially spiral in and form the nuclei. Thus, the innermost GCs are younger with higher metal enrichment than the outer GCs that continue to orbit after the nuclei formation. Our findings are consistent with previous literature on galaxy formation. Observation of galaxies in general (not only dEs) and galaxy formation theories find that galaxies tend to have age and metallicity gradients; the inner regions of galaxies are younger and metal-rich than the outer regions (Brown et al. 2005, Fardal et al. 2009). If dynamical friction is discovered to not occur in dEs, then the parameter we established still needs to be explored because there could be a separate episode of nuclei formation after the development of GCs and dE halos as described in Lotz et al. (2004).

3.2 Comparing Chemical Compositions of Satellite and Orphan GCs

We used the previous techniques and absorption lines to compare satellite and orphan GCs. From Figure 10A, the orphan GCs are younger than the satellite GCs because they have stronger H-alpha lines. Orphan GCs also have higher metallicities than satellite GCs because they show stronger CaT lines in Figure 10B. Stronger magnesium, magnesium triplet, and sodium doublet lines corroborate our CaT findings. These results suggest the orphan GCs we studied have a younger mean age and higher average metal concentrations than the GCs orbiting dEs in Virgo. If these orphan GCs are bounded to large ellipticals in Virgo such as M87, then our findings are not surprising; in cluster environments, dwarf galaxies are more susceptible to ram pressure and tidal stripping (Mayer et al. 2006). Thus, the GCs orbiting larger galaxies most likely coalesce from more metal enriched gas than the GCs orbiting dEs.

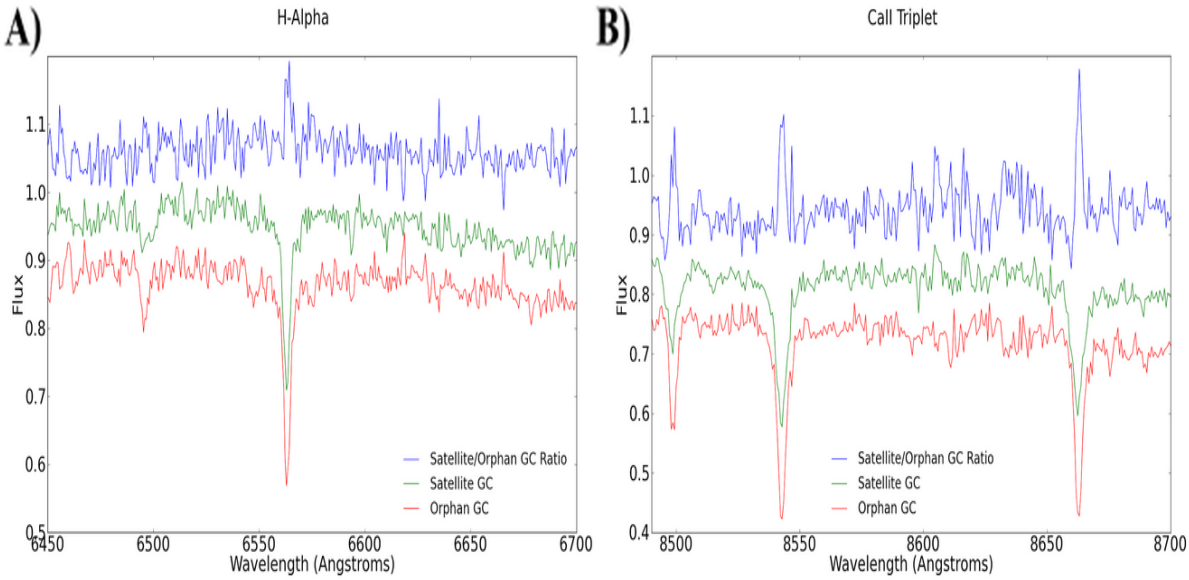

Figure 10: H-Alpha and Ca Triplet Absorption Lines for Satellite and Orphan GCs. In 10A, a stronger H-alpha line in the orphan GC spectra suggests that they are younger than GC bounded to dEs. The orphan GCs also have higher metallicities because they have stronger CaT absorption lines shown in 10B.

4. Conclusion and Future Work

This study was the first to compare the co-added spectroscopic data and absorption lines of 19 dwarf elliptical galaxy nuclei and 83 globular clusters orbiting dEs in Virgo, finding that the nuclei are younger and more metal rich. Our results function as important parameters for dE formation theories such as dynamical friction because the stars that constitute the nuclei most likely formed later than the stars in the satellite GCs.

In the future, we will obtain photometric data of the stars and GCs in bands of light redder than far red z band to better separate our globular cluster and foreground star sample. Literature has shown that GCs and foreground stars stratify into sequences much better in color-color space with redder filters such as J, H , and K (Muñoz et al. 2014). A better separation of these objects will allow us to better analyze the contamination in both data sets.

Our spectral comparisons have been predominantly qualitative; that is, we make conclusions based on any spikes or dips in the ratio between the two spectra. We will conduct a more quantitative analysis by numerically measuring the age and metallicity of dE nuclei and their satellite GCs. Moreover, we will compare our co-added spectra to models created by the stellar population synthesis (SPS) technique. SPS models are essential linchpins that use continually improving stellar formation theories to connect observational data to theory. A very useful aspect of these models is that they were created to simulate the effects of certain parameters on galaxy formation. The age, chemical concentrations, and other factors can be tweaked to analyze the corresponding effects on the synthetic spectra with respect to the observational spectra. We will compare SPS models from literature such as Bruzual & Charlot (2003), Maraston (2005), and Vazdekis et al. (2010) with our co-added dE nuclei and GC spectra.

Finally, we will examine our orphan GC sample more comprehensively. These GCs are especially interesting because if they are remote satellites of the massive elliptical M87, they

would be the most distant confirmed GCs in any galaxy. For further inspection, we will plot their radial velocity distribution and determine their velocity dispersion. If the velocity distribution is symmetric around the mean velocity of M87 and the velocity dispersion is similar to that of M87, then these GCs are the farthest confirmed satellites of this massive elliptical. The velocity dispersion results can then be used as constraints on the dark matter halos of M87.

Dwarf elliptical galaxies are important areas of study because of their abundance in the Universe and their role in shaping galaxy formation. Thus, learning more about the formation of dE nuclei and their orbiting GCs is necessary before we can completely understand the origins of other galaxies and life in the Universe.

References

Bender, R., Burstein, D., & Faber, S. 1992, AJ, 399, 462

Binggeli, B., Sandage, A., & Tammann, G. 1988, ARA&A, 26, 509

Binggeli, B., Sandage, A., & Tammann, G. 1985, AJ, 90, 1681

Brown, T. M., Ferguson, H. C., Smith, E., et al. 2005, AJ, 130, 1693

Bruzual, G., & Charlot, S. 2003, MNRAS, 344, 4

Cenarro, A. J., Gorgas, J., Vazdekis, A., et al. 2003, MNRAS, 339, L12

Côté, P., Blakeslee, J. P., Ferrarese, L., et al. 2004, ApJS, 153, 223

Côté, P., Piatek, S., Ferrarese, L., et al. 2006, ApJS, 165, 57

Dressler, A., 1980, ApJ, 236, 351

Fardal, M., Guhathakurta, P., Gilbert, K., et al. 2009, ASP Conf. Ser., 419

Ferguson, H., & Binggeli, B. 1994, A&A, 6, 67

Ferrarese, L., et al., 2012, ApJS, 200, 4

Lotz, J. M., Miller, B. W., & Ferguson, H. C. 2004, ApJ, 613, 262

Maraston, C., 2005, MNRAS, 362, 3

Mayer, L., Mastropietro, C., Wadsley, J., et al. 2006, MNRAS, 369, 1021

Muñoz, R. P., Puzia, T. H., Lançon, A., et al., 2014, ApJS, 210, 4

Oh, K. S., Lin, D. N. C., & Richer, H. B. 2000, ApJ, 531, 727

Peng, E. W., Jordán, A., Côté, P., et. al. 2006, ApJ, 639, 95

Schiavon, R.P., Barbuy, B., Rossi, S. C. F., & Milone, A. 1997, ApJ, 479, 902

Tantolo, R., & Chiosi, C. 2004, MNRAS, 353, 917

Terlevich, E., Diaz, A. I., & Terlevich, R. 1990, MNRAS, 242, 271

Toloba, E., Boselli, A., Cenarro, A. J., et. al. 2011, A&A, 526, A114

Toloba, E., Boselli, A., Gorgas, J., et. al. 2009, ApJL, 707, 1

Toloba, E., Guhathakurta, P., van de Ven, G., et. al. 2014, ApJ, 783, 2

van Dokkum, P., & Conroy, C. 2011, ApJL, 735, L13

Vazdekis, A., Sánchez-Blázquez, P., Falcón-Barroso, J., et. al. 2010, MNRAS, 404, 4

Worthey, G., Faber, S. M., Jesús González, J., et al. 1994, ApJS, 94, 687